Critical contribution of endothelial protein C receptor in experimental malaria-associated acute respiratory distress syndrome

Luana dos Santos Ortolan[1,#,*], Michelle Klein Sercundes[2], Gabriel Candido Moura[2], Thatyane de Castro Quirino[2], Daniela Debone[2], Douglas de Sousa Costa[3], Oscar Murillo[3], Claudio Romero Farias Marinho[3], Sabrina Epiphanio[1,2].

Authors Affiliations:

[1]Departmento de Imunologia, Instituto de Ciências Biomédicas, Universidade de São Paulo, São Paulo, Brazil.

[2] Departamento de Análises Clínicas, Faculdade de Ciências Farmacêuticas, Universidade de São Paulo, São Paulo, Brazil.

[3] Departamento de Parasitologia, Instituto de Ciências Biomédicas, Universidade de São Paulo, São Paulo, Brazil.

[#] Current address: Department of Dermatology, Carver College of Medicine, University of Iowa, Iowa City, Iowa, United States.

Corresponding author:

*E-mail: luana_ortolan@yahoo.com.br (LSO)

Keywords: malaria; endothelial cells, cytoadherence; *Plasmodium berghei* ANKA; ARDS; adhesion molecule; EPCR

Abstract

Plasmodium falciparum malaria severity is associated with parasite cytoadherence, but limited knowledge about its effect in malaria-associated acute respiratory distress syndrome (ARDS) is notorious. Our objective was to evaluate cytoadherence of infected red blood cells (iRBC) in a murine model of ARDS and appraise the role of endothelial protein C receptor (EPCR) in ARDS pathogenesis. Lungs from ARDS-developing mice showed evidences of iRBC accumulation in lungs besides increase of EPCR and TNF concentrations. Furthermore, TNF increased iRBC adherence *in vitro*. Dexamethasone-treated infected mice showed lower levels of TNF and EPCR mRNA expression and, finally, decreased the vascular permeability, protecting mice from ARDS. In addition, EPCR knockdown decreased the capacity of iRBC adherence *in vitro*. In conclusion, we identified that increased iRBC cytoadherence in lungs underlies malaria-associated ARDS in DBA/2 infected mice and that inflammation increased cytoadherence capacity through EPCR expression suggesting a potential target for drug development.

Author summary

It's important to understand the development of malaria-associated acute respiratory distress syndrome (ARDS) to help in better prognosis and therapy. Carrying out a model using rodents suffering from ARDS, which is similar to that in humans, we were able to report, *in vivo* and *in vitro* approaches, that *P. berghei* ANKA, a parasite from mice, adhere in lungs endothelial cells of infected mice. We show that a receptor

named EPCR is important in this adhesion. This receptor is modulated by TNF, an pro-inflammatory factor, being decreased by dexamethasone, an anti-inflammatory drug. This treatment, which improves the infected mice respiratory parameters and lung lesions, due to less adherence, inflammation and pulmonary vascular permeability, could be considered as a co-treatment with antimalarial drugs.

Introduction

Malaria infections by *Plasmodium falciparum* are responsible for the largest number of severe and fatal cases in the tropics [1,2]. The main complications of *P. falciparum* include cerebral malaria, pulmonary complications, acute renal failure, severe anemia, bleeding and placental malaria [3]. An important aspect of the pathogenesis of severe malaria results from the ability of infected red blood cells (iRBC) to adhere in the microvasculature. This interaction between the iRBC and the endothelium can cause blocking blood flow and/or local inflammatory response [3–5]. Furthermore, these adhesions promote the disappearance of asexual forms of the parasite in the peripheral circulation, thus, preventing them from being destroyed in the spleen [3,5,6]. Pulmonary complications caused by severe malaria include Acute Respiratory Distress Syndrome (ARDS), which has been associated with different diseases and not only being a result of severe malaria [7–9]. Even though malaria-associated ARDS often causes high mortality rate, slight research has been done. Murine models have been used to study malaria-associated ARDS [10,11] and DBA/2 mice infected with *P. berghei ANKA* (PbA) develop ARDS and die between the 7th to 12th days post infection (dpi) without signals of cerebral malaria. In addition, we established a predictive criteria to distinguish which mice would die from ARDS, on the 7th dpi, using respiratory and parasitemia date [12]. Using this model, we found that

71 recruitment of neutrophils and VEGF are essential to the pathogenesis of malaria-
72 associated ARDS [13,14] and the induction of heme oxygenase-1 (HO-1) has a
73 protective effect in the development of ARDS in mice [15].
74 Additionally, it has already been demonstrated that PbA-iRBC adhere to MVECS
75 (microvascular lung endothelial cells from CBA/Ca mice) and that TNF-stimulated cells
76 express more ICAM-1 and VCAM [16]. In *P. chabaudi* model, the absence of ICAM-1
77 in infected mice, showed less anemia and weight loss, reduced parasite accumulation in
78 both spleen and liver and higher peripheral blood parasitemia during acute stage
79 malaria, which presented the slight importance of ICAM-1 in adhesion and
80 pathogenesis of *P. chabaudi* [17].
81 Endothelial receptors have been studied to understand the iRBC adherence in the
82 microvasculature of different organs in severe malaria and some of these receptors are
83 well established such as ICAM-1 in cerebral malaria and CSA in placental malaria [18].
84 However, both the adhesion and consequences of PbA-iRBC into DBA/2 lung
85 endothelial cells remains unknown. In 2013, Endothelial protein C receptor (EPCR)
86 was shown to be a new receptor for *Plasmodium falciparum* erythrocyte protein 1
87 (PfEMP1) in *P. falciparum* severe malaria [19] which may result in a new branch of
88 research in severe malaria. EPCR has, as its primary function, to bind with activated
89 protein C (APC) and to cleave protease activated receptor 1 (PAR-1), in a specifically
90 RAC1 pathway, which inhibits the activation of the nuclear factor-κβ and provides
91 barrier protection [20]. EPCR facilitates the activation of protein C (PC) by the
92 thrombin-thrombomodulin complex; the cytoprotective effects of EPCR results in
93 vascular and tissue protection in brain, lungs, kidneys and liver [21]. Also, APC
94 cytoprotective activities provide neuroprotective effects as anti-inflammatory and anti-
95 apoptotic, protecting the blood-brain barrier, kidneys and lungs, and thus, may be

96 directly relevant to the complications associated with severe malaria [22]. Indeed, in
97 vitro studies with purified CIDRα1 domains and iRBCs with selected *P. falciparum*
98 laboratory strains confirm the loss of EPCR functionality upon CIDRα1 or iRBC
99 binding that includes loss of PC and APC binding to EPCR, inhibition of EPCR-
100 mediated PC activation and obstruction of APC-mediated endothelial barrier protective
101 effects. Consequently, the binding of PfEMP1 to EPCR results in an acquired functional
102 PC system deficiency which supports new evidences that EPCR plays a central role in
103 the pathogenesis of severe malaria [22]. EPCR binding is mediated through the amino-
104 terminal cysteine-rich interdomain region (CIDRa1) of DC8 and group PfEMP1
105 subfamilies, and that CIDRa1 interferes with protein C binding to EPCR [23].
106 However, it has unexpectedly been shown that parasitized erythrocytes expressing the
107 DC13 HB3var03 or IT4var07 variants of PfEMP1 do not bind to the EPCR of brain
108 endothelial cells in vitro. On the other hand, it has been evidenced that the DC8 variant
109 IT4var19 may bind to the EPCR, but this interaction was inhibited when standard
110 human serum or plasma was added to the assays. Therefore, the discrepancy in the
111 binding activity of the EPCR and the recombinant PfEMP1 proteins indicates the need
112 for further studies to understand the current physiological significance resulting from
113 this PfEMP1-EPCR interaction [24].
114 Although there are some suggestions that PfEMP1 can bind to EPCR with important
115 effects on the severe malaria, these data are controversial, and, in addition, there are any
116 evidences of *P. berghei* ANKA binding on EPCR and the effects of EPCR on ARDS
117 pathogenesis must be elucidated. Our study herein was developed in a murine model,
118 which mimics various human ARDS, [12] and used primary culture of microvascular
119 lung endothelial cells from DBA/2 mice (PMLEC), to clarify not only the adhesion of
120 infected erythrocytes to murine lung microvascular endothelial cells, but also

121 understand the relevant aspects of EPCR modulation by the immune response which
122 can bring important contribution to understand malaria-associated ARDS.

123

124 ## Results

125 **ARDS-developing mice show higher load pulmonary parasite than HP-developing**
126 **mice**

127 In our previous study, it was shown that a proportion of DBA/2 mice infected with
128 PbA-iRBC developed singular characteristics of ARDS and died between the 7th and
129 12th dpi [12–15]. To investigate if adherence is essential in the evolution of this
130 phenotype, we observed that PbA-luciferase-infected erythrocytes were distributed in
131 the peripheral blood and tissues of DBA/2 mice. However, when they were perfused
132 with PBS 1x, the bioluminescence (luciferase/luciferin) signal remained concentrated
133 in spleen and lungs, especially in ARDS-developing mice (Fig 1 A-C), corroborating
134 with our published data [14]. We demonstrated that ARDS-developing mice showed
135 higher levels of *18s* subunit PbA rRNA expression (Fig 1D) and higher hemozoin
136 concentration in the lungs compared to HP-developing mice, on the 7th dpi (Fig 1 E-G).
137 In addition, we analyzed histological lung section of ARDS-developing mice, finding
138 several iRBC in close contact with endothelial cells (Fig 1H). These results together
139 indicated that ARDS-developing mice accumulated a considerable amount of infected
140 red blood cells (iRBC) in the lungs, suggesting the essential participation on ARDS
141 pathogenesis.

142

143 **TNF increases *Plasmodium berghei* adherence in ARDS experimental model**

144 ARDS-developing mice, on the 7th dpi, displayed higher TNF levels in serum compared
145 to HP-developing mice (Fig 2A), suggesting that this inflammatory cytokine may be
146 critical to ARDS development. For this, we further investigated if iRBC could
147 contribute to TNF release by endothelial cells. First, we demonstrated that PMLEC
148 stimulated with iRBC can directly contribute to TNF production (Fig 2B). Then, we
149 checked the influence of TNF in adhesion of iRBC in PMLEC through static and flow
150 conditions. It was observed that TNF-stimulated cells increased the capacity of iRBC
151 adherence into PMLEC after 24 and 72 hours in static assay (Fig 2 C-E). In the flow
152 adherence assay, which mimics the physiologic conditions, the iRBC had more
153 cytoadherence with TNF than without TNF stimulation (Fig 2 F-H). In addition,
154 PMLEC were seeded in transwell plates in indirect contact with peritoneal macrophages
155 (Mφ), stimulated or not by red blood cells (RBC) or iRBC (Fig 2I). Mφ stimulated by
156 iRBC produced more TNF than Mφ without previous contact with iRBC (Fig 2J). These
157 Mφ also produced IFN-γ and IL-10 but with no difference between groups (data not
158 shown). Additionally, PMLEC that was submitted to indirect contact with Mφ
159 stimulated with iRBC demonstrating more adherence of iRBC than PMLEC with no
160 previous contact with Mφ (Fig 2K). Finally, in order to evaluate the contribution of
161 TNF in the adhesion of iRBC in PMLEC, cells were blocked with TNF antibody and, as
162 a result, the blockage reduced the capacity of iRBC to adhere in PMLEC (Fig 2L). All
163 these data show that ARDS-developing mice have more TNF, which contributes to
164 iRBC adherence in endothelial cells than in HP-developing mice.
165

166 **EPCR acts directly in *P. berghei* cytoadherence**

167 Looking for adhesion molecules that could be involved in PbA-iRBC cytoadherence in
168 ARDS pathogenesis, we observed that ARDS-developing mice showed higher levels of
169 VCAM and ICAM-1 in lungs than HP-developing or non-infected mice (NI), analyzed
170 by immunohistochemistry (Fig S2 A-C). Also, recombinant TNF upregulated the
171 mRNA expression of ICAM-1 and VCAM in PMLEC (Fig S2 D-I).
172 However, the most interesting findings were the mRNA EPCR expression upregulated
173 in the lungs of ARDS-developing mice compared to NI mice (28.48-fold increase) and
174 HP-developing mice (13.16-fold increase) (Fig 3A). There was also an increase in
175 soluble EPCR (sEPCR) (Fig 3B) and EPCR protein (Fig 3C) in ARDS-developing mice
176 serum compared to HP-developing mice. We further investigated the influence of TNF
177 in the regulation of EPCR expression in PMLEC. TNF-stimulated cells showed an
178 upregulation in EPCR expression in 48 and 72 hours, but not with PbA-iRBC stimulus
179 (Fig 3 D-F). Moreover, EPCR knockdown with siRNA transfection in PMLEC, reduced
180 EPCR expression compared to non-stimulated PMLEC (Fig 3G) and reduced the
181 adherence of iRBC (Fig 3H), suggesting an important contribution of TNF and EPCR to
182 adherence of iRBC in PMLEC.
183

184 **Dexamethasone reduces TNF and EPCR, protecting mice lungs and PMLEC from**
185 **increased vascular permeability**

186 Once TNF seems to be important to induce PbA-iRBC adherence, and consequently,
187 ARDS development, DBA/2 mice were infected with PbA-iRBC and treated with
188 dexamethasone (80 mg/kg) to investigate if it could protect them from lung injury.
189 Dexamethasone treatment decreased TNF concentrations (Fig 4A) apart from IL-6 and
190 IL-33 concentrations in treated mice, compared to non-treated mice (Fig S3 A and B).
191 Dexamethasone also downregulated EPCR expression in lungs of infected mice (Fig

192 4B) and sEPCR concentration in serum and bronchoalveolar lavage (BAL) (Fig 4C and
193 D). VEGF concentration, an essential factor to increase vascular permeability and
194 ARDS development, also decreased after dexamethasone treatment in the BAL of
195 infected mice, on the 7th dpi (Fig 4E).
196 Consequently, we analyzed the lung vascular permeability and dexamethasone-treated
197 infected mice showed to be protected compared to non-treated mice (Fig 4F-H). To
198 clarify the mechanism that reduced the lung permeability, the opening of
199 interendothelial junctions in PMLEC through actin analyzes was evaluated. The
200 PMLEC stimulated with iRBC increased the spaces between the interedothelial
201 junctions and leads to the disruption and reorganization in the actin filaments which was
202 protected by the treatment with dexamethasone (Fig 4I and J). iRBC-stimulated
203 PMLEC also demonstrated more permeability of Evans Blue in a transwell assay,
204 compared to dexamethasone-treated PMLEC (Fig 4K). Additionally, dexamethasone-
205 treated PMLEC showed a reduction in VEGF concentration compared to cells not
206 treated with dexamethasone (Fig 4L). Everything considered, these data suggest that
207 dexamethasone is capable to reduce inflammation, decreasing EPCR and vascular
208 permeability in PMLEC and lungs of DBA/2 mice.
209
210 **Anti-inflammatory drug protects mice from ARDS but not from malaria infection**
211 Dexamethasone-treated mice improved their respiratory parameters [Respiratory
212 Frequency, Tidal Volume and Enhanced Pause (Penh)] compared to infected non-
213 treated mice, on the 7th dpi (Fig 5 A-C). On the other hand, parasitemia levels increased
214 in peripheral blood in dexamethasone-treated mice on the 7th dpi (Fig 5D) and these
215 mice succumbed between 8 and 20 dpi with characteristics of HP, without edema and
216 lower inflammatory infiltration according to the histopathological and count of iRBC

217 data (Fig 5 D-G). Finally, we proposed the essential mechanisms of protection of
218 dexamethasone in experimental malaria (Fig 6) suggesting that PbA-iRBC induce TNF
219 release by endothelial cells and by Mφ, then the TNF up-regulates EPCR expression in
220 PMLEC, increasing the iRBC adhesion through EPCR pathway. The adhesion of iRBC
221 in PMLEC leads to gap formations increase in the interendothelial junction, raising
222 vascular permeability and consequently, edema formation. Activated alveolar
223 macrophages also produce TNF, which contributes to the activation of endothelial cells,
224 possible recruitment of neutrophils [14] and alveolar damage. The drastic reduction in
225 inflammation with dexamethasone may be responsible for the increase in parasitemia
226 and mortality. All things considered, these data suggest that TNF is essential to increase
227 expression of EPCR and consequently, increase adhesion of iRBC in malaria-associated
228 ARDS.
229

230 **Discussion**

231 We describe, in the present study, the cytoadherence of PbA-iRBC in microvascular
232 lungs endothelial cells in mice which develop ARDS as well as the importance of the
233 EPCR in this mechanism and, consequently, in the ARDS pathogenesis.
234 A relevant advantage of this study is that our animal model reproduces
235 physiopathological aspects from those found in human ARDS [12,13,25]. Moreover, the
236 pathogenesis of ARDS in this experimental model is only related to pulmonary
237 manifestation development, because there are no inflammatory signs associated to
238 cerebral malaria [13], differently from what occurs in some other animal models [26]. It
239 is also important to note that most ARDS-associated malaria models have their
240 syndrome aspects compared with those in non-infected mice. Here, we compared

241 aspects of ARDS mice with those also infected but had not developed the syndrome and
242 died from hyperparasitemia and anemia.
243 It is well known that mature forms of *P. falciparum*-iRBC can adhere to the
244 microvasculature of different organs which is an important feature in the pathogenesis
245 of severe malaria in humans [5,27]. Animal models have been used to study severe
246 malaria pathogenesis which is well established, especially for cerebral malaria [28].
247 However, as there are just few studies focusing ARDS murine models [11,26], the
248 pathogenesis is not completely enlightened. Recently, PbA-iRBC has been
249 demonstrated, *in vitro,* to adhere to MVECS (microvascular lung endothelial cells from
250 CBA/Ca mice) and that TNF-stimulated cells have expressed more ICAM-1 and VCAM
251 [16], and in our results. Nonetheless, there are not studies about the expression of EPCR
252 in acute respiratory distress syndrome in human beings or murine malaria. It is known
253 that iRBC adhere to endothelial cells, *in vivo* and *in vitro.* Nevertheless, the study herein
254 is the first showing PbA-iRBC adherence using DBA/2 mice that developed ARDS.
255 Additionally, our findings provide the first evidence that PbA-iRBC adhere more in
256 ARDS-developing mice than in those HP-developing. Moreover, we found that ARDS-
257 developing mice have about 28.5 times more EPCR expression than those not infected,
258 implying that EPCR can be essential in ARDS progress. Finally, we demonstrated that
259 TNF-stimulated cells induced EPCR expression while iRBC did not.
260 Previously, we had found that ARDS-developing mice showed more parasites load in
261 lungs, which can be important to induce the syndrome, than those HP-developing. On
262 the other hand, it is mostly unknown whether the parasite can directly induce ARDS
263 development or not.
264 Quite a few works have been presenting the adherence of PbA Luciferase (PbAluc) *in*
265 *vivo* [29,30] and our work reinforces it. The PbAluc-iRBC was accumulated in the

266 lungs of DBA/2 mice, especially in those ARDS-developing, when the organs were
267 perfused we confirmed that the PbA-iRBC was adhered mainly in the lungs and spleen.
268 On the other hand, in our experimental model, there was no adhesion in the brain as in
269 other models of ARDS [11,26].
270 Also, ARDS-developing mice showed more hemozoin (Hz) area in lungs compared to
271 those HP-developing on the 7th dpi, the onset of ARDS development, and some previous
272 works suggest that Hz, which is released from the food vacuole into circulation during
273 erythrocyte lysis is rapidly taken up by circulating monocytes and tissue macrophages,
274 inducing the production of pro-inflammatory mediators [31,32]. In addition Hz linked
275 by *Plasmodium* DNA is a ligand for TLR 9, which activates innate immune responses *in*
276 *vivo* and *in vitro*, resulting in the production of cytokines, chemokines, and up-
277 regulation of costimulatory molecules [33,34] and proinflammatory mediators like IL-
278 1β, via NLP3 inflammasome complex activation [32].
279 Interestingly, due to the fact that some mice develop ARDS and others do not, and HP-
280 developing mice also had some Hz and parasite adhered in lungs, we further
281 investigated the adhesion of PbA-iRBC in endothelial cells with different stimuli. Other
282 studies show that endothelial cells stimulated with TNF had an increase in ICAM-1
283 expression [35,36], corroborating with our results *in vivo* and *in vitro*, as recently
284 demonstrated that TNF and ICAM-1 markers were increased in the lungs of the patients
285 who developed the syndrome [37]. It is interesting to highlight that the parasites by
286 themselves (PbA-iRBC or PbA-iRBC extract) cannot upregulate the ICAM-1, VCAM
287 or EPCR expression in DBA/2-PMLEC. Actually, PbA-iRBC adhere more in TNF-
288 stimulated DBA/2-PMLEC.
289 With the hypothesis that inflammation is essential to expose adherence molecules and
290 consequently ARDS pathogenesis, we treated DBA/2 mice with dexamethasone to

291 reduce inflammation, observing that these mice were protected from ARDS and had a
292 downregulation in EPCR expression, which indicates that EPCR may be important to
293 iRBC adherence and to the pathology progress of the disease. However, in a recent
294 study, the expression of EPCR decreased in the lungs of *P. falciparum*-infected patients
295 who developed ARDS when compared to those who did not develop, analyzed by
296 immunohistochemistry. Although, the authors suggest that the change in EPCR,
297 together with thrombomodulin in association with the deposition of hemozoin in the
298 lungs, play an important role in the pathogenesis of ARDS [37]. Besides that,
299 dexamethasone-treated mice are less susceptible to increase the vascular permeability.
300 Likewise, iRBC-stimulated PMLEC and treated with dexamethasone showed lesser
301 permeability compared to not treated cells. These results are similar to those found in an
302 experimental model of C57bl/6 mice infected with *P. berghei* NK65 and treated with
303 the same dose of dexamethasone. The authors showed an increase in the peripheral
304 parasitemia and ARDS protection [26], but not an effect in the pulmonary vascular
305 permeability. On the other hand, the increase in vascular permeability was previously
306 found in our ARDS model [12].
307 *P. falciparum*-infected patients present elevated levels of circulating nitrogen oxide
308 reactive intermediates and by cytokines, such as IFNα/γ, TNF, IL-1, IL-6, and the
309 chemokine IL-8. Furthermore, these cytokines and chemokines levels have been found
310 to correlate with different manifestations of severe malaria [32]. Additionally, although
311 ARDS of different etiologies is characterized by a local inflammatory response, the
312 inflammatory mediators can spread into the general circulation. The severity of ARDS
313 depends on of the magnitude of the resultant systemic inflammatory response [38].
314 Based on our results, the treatment with dexamethasone, a potent anti-inflammatory
315 drug, decreased the serum concentrations of IL-33, IL-6 and TNF in PbA-infected mice.

316 IL-33 is a tissue-derived nuclear cytokine from the IL-1 family and it's highly expressed
317 during homeostasis and inflammation in endothelial, epithelial and fibroblast-like cells,
318 working as an alarm signal released upon cell injury or tissue damage to alert immune
319 cells to express the ST2 receptor (IL-1RL1). The major targets of IL-33 *in vivo* are
320 tissue-resident immune cells such as mast cells, group 2 innate lymphoid cells (ILC2s)
321 and regulatory T cells (Tregs). IL-33 is emerging as a crucial immune modulator in
322 regulatory immune responses and infectious inflammatory diseases [39]. Bronchial IL-
323 33 expression is significantly increased in severe malaria patients with pulmonary
324 edema [40]. Moreover, in PbA-induced experimental cerebral malaria (ECM), IL-33
325 expression is increased in brain, and ST2-deficient mice were resistant to PbA-induced
326 neuropathology [41,42]. On the other hand, another publication demonstrated that PbA-
327 infected C57BL/6 mice treated with recombinant IL-33 presented no signs of
328 neurological pathology associated with CM and had reduced production of pro-
329 inflammatory cytokines and chemokines[43].
330 The IL-6-type cytokines are released in response to tissue injury and/or an inflammatory
331 stimulus. They act locally and systemically to generate a variety of physiologic
332 responses, especially in the acute phase response [44]. Circulating IL-6 levels are
333 elevated in nearly all infectious, traumatic, and inflammatory states including ARDS.
334 Elevated levels of IL-6 are found in BAL and plasma of patients with ARDS and those
335 at risk [45,46]. Finally, the TNF is an inflammatory mediator strongly implicated in the
336 development of ARDS [47], signal through two receptors, p55 and p75, which play
337 differential roles in pulmonary edema formation during ARDS. It was shown that p55
338 by a novel domain antibody (dAb™) attenuated ventilator-induced lung injury [48] and
339 also lung injury and edema formation in models of ARDS induced by acid aspiration
340 [47]. Recently, a selective blockage of TNFR1 (GSK1995057 antibody) inhibited

341 cytokine and neutrophil adhesion molecule expression in activated HMVEC-L
342 monolayers *in vitro* and attenuated inflammation and signs of lung injury in primates.
343 Moreover, treatment with this antibody attenuated pulmonary neutrophilia,
344 inflammatory cytokine release and signs of endothelial injury in BAL and serum sample
345 in healthy humans challenged with a low dose of inhaled endotoxin [49].
346 In conclusion, our data suggest that *P. berghei* infection induces TNF production by
347 inflammatory and endothelial cells, leading to the expression of adhesion molecules,
348 such as ICAM-1, VCAM and, especially EPCR. These results allow us to infer that
349 those factors are essential for PbA-iRBC cytoadhesion, and, thus, strongly suggest the
350 participation of these mechanisms in the pathogenesis of malaria-associated ARDS.
351 Being known that inhibition of cytoadhesion mechanisms may improve the prognosis of
352 infection [50], we emphasize that the processes described above may be important
353 targets in the treatment of ARDS due to *Plasmodium* infection, acting as adjunctive
354 therapy in association with the use of antimalarials, not only making the treatment more
355 efficient, but also reducing the morbidity and mortality of these patients.

356

357 # Methods

358

359 **Experimental outline**

360 Ten to twelve DBA/2 mice per group were infected with 10^6 infected red blood cells
361 (iRBC) of *Plasmodium berghei* ANKA (PbA).
362 To classify PbA-infected mice in ARDS-developing or HP-developing before the death,
363 on the 7th dpi, we used parameters such as respiratory patterns (enhanced pause and

364 respiratory frequency) and parasitemia as predictive, according to previously described
365 [12]. Lung tissue, blood and BAL samples were collected from mice on the 7th day post
366 infection (dpi).
367
368 **Ethics statement**
369 All experiments were performed in accordance with the ethical guidelines for
370 experiments with mice, and the protocols were approved by the Animal Health
371 Committee of the Biomedical Sciences Institute of the University of São Paulo (CEUA
372 nº 24, page 16, book 03). The guidelines for animal use and care were based on the
373 standards established by National Council for Control of Animal Experimentation
374 (CONCEA: Conselho Nacional de Controle de Experimentação Animal), The Brazilian
375 College of Animal Experimentation (COBEA) and Brazilian Federal Law nº 11.794.
376 Infected mice were monitored daily and euthanized with (150 mg/kg)/xylazine (15
377 mg/kg) when they presented any symptoms of suffering. Animals for the
378 experimentation were euthanized with ketamine and xylazine on the 7th after infection
379 according to the approved ethics committee.
380
381 **Mice, parasites and euthanasia**
382 Male DBA/2 mice between 6-10 weeks old (purchased from the Department of
383 Parasitology, University of São Paulo, Brazil) were infected with $1x10^6$ *P. berghei*
384 ANKA (clone 1.49L) iRBCs, as previously defined [12]. Parasitemia and mortality
385 were monitored daily. Parasitemia was determined by Giemsa staining and expressed as
386 the percentage of infected red blood cells. The euthanasia of mice was made using
387 ketamine (150 mg/kg)/xylazine (15 mg/kg).
388

389 **Determination of Respiratory Pattern**

390 Respiratory patterns (respiratory frequency [RF], tidal volume [TV] and enhanced
391 pause [Penh]) were monitored on the 7th dpi by an unrestrained whole-body
392 plethysmography chamber (WBP, Buxco Electronics, USA) for 10 minutes (basal
393 level), according to formerly described [12].

394

395 **Histopathological analyses and hemozoin count**

396 Lung tissue fragments were fixed with 10% buffered formalin for 24 hours and kept in
397 70% ethanol until embedding in paraffin and 4–5 μm sections were stained with
398 hematoxylin-eosin (HE). To perform the count of hemozoin (Hz) area, lungs of mice
399 euthanized (ARDS-developing or HP-developing mice, on the 7th day after-infection
400 according to the predictive model [12]) were stained with H&E, 10 images were
401 captured from each tissue using polarized light (400x magnification) using a Zeiss
402 color camera (cam Axio HRc), connected to a light microscope Zeiss (Axio Imager
403 Program. M2). The corresponding percentage of Hz in each image area was identified
404 using the program Image J in which the points of Hz were distinguished by brightness
405 adjustment.

406

407 **Quantification of gene expression**

408 Quantitative RT-PCR was performed for relative quantification of gene expressions
409 from lungs of non-infected and infected mice. RNA extraction was performed according
410 to the "Animal Cell I" protocol from RNeasy Mini (Qiagen, USA). cDNA synthesis was
411 performed with 1μg RNA sample, using First Strand cDNA Synthesis kit RT-PCR
412 (Roche, USA) according to manufacturer's instructions. Finally, to gene expression,
413 SYBR Green PCR Master Mix (Applied Biosystems, USA) and relative quantification

414 2 $^{(-\Delta\Delta CT)}$ method were used as described before (51). The qRT-PCR reactions were
415 performed in the 7500 Fast instrument (Applied Biosystems, USA) using
416 oligonucleotides: PbA 18s (forward 5'-agcattaaataaagcgaatacatccttac-3'; reverse 5'-
417 ggagattggttttgacgtttatgtg-3'); HPRT (forward 5'-aagcttgctggtgaaaagga-3'; reverse 5'-
418 ttgcgctcatcttaggcttt-3'); ICAM-1 (forward 5'-cgaaggtggttcttctgagc-3'; reverse 5'-
419 gtctgctgagscccctcttg-3'); VCAM (forward 5'-agtccgttctgaccatggag-3'; reverse 5'-
420 tgtctggagccaaacacttg-3'); EPCR (forward 5'-gacgaagtttctgccgctac-3'; reverse 5'-
421 ctggaggatggtgacgtttt-3'); TNF (forward 5'-aatggcctccctctcatcagtt-3'; reverse 5'-
422 ccacttggtggtttgctacga-3').
423
424 **Parasite localization by bioluminescence**
425 DBA /2 mice were infected with *P.berghei* ANKA expressing luciferase. On the 7th day
426 post-infection, luciferin (VivoGlo ™ Luciferin, In Vivo Grid, Catalog #: P1041,
427 Promega) was injected allowing the emission of parasite luminescence. Then the
428 localization of the parasite was analyzed with IVIS Spectrum (PerkinElmer). For this
429 purpose, mice were sedated with isoflurane for pictures (approximately 6 minutes after
430 the injection of luciferin). Later, they were euthanized and perfused. After the perfusion,
431 a new image of the mice was captured, the organs were collected and placed in sterile
432 petri dishes for observation of bioluminescence of each tissue.
433
434 **Cytokines quantification**
435 The quantities of TNF, IL-6, IL-33 in serum and culture supernatants were determined
436 by ELISA commercial kits eBioscience (San Diego, CA, USA) *mouse Elisa Ready-Set-*
437 *Go*: TNF (ref 88-7324-88), IL-6 (ref 88-7064-88) and IL-33 (ref 88-7333-88), according to the
438 manufacturer protocols.

439

440 **Isolation of the primary microvascular lung endothelial cells**

441 Primary microvascular lung endothelial cells (PMLEC) were obtained from DBA/2
442 mice, as described before (15,52),. Briefly, after euthanasia, the animal body was
443 disinfected with iodine alcohol. Then, the mice had all its blood taken by cutting the
444 carotid artery. In a laminar flow chamber, the lung tissue was cut into fragments of
445 approximately 1mm^2 and distributed among 6-well polystyrene plates in 20% of fetal
446 bovine serum (FBS) and antibiotics supplemented DMEM culture medium at 37°C and
447 5% CO_2. After, 72 h, the tissue fragments were removed and 50% of the medium was
448 replaced. After 7 days of incubation, the cells were removed with trypsin 0.25% EDTA
449 (Gibco) and replaced in a 75 cm^2 culture flask. The trypsinization procedure was
450 repeated every 5 to 7 days. Finally, the cells were cultured for 15 to 20 days (3rd and 4th
451 passage) until being used in the trials. The isolated DBA/2-PMLEC were characterized
452 by immunofluorescence with Lectin from *Ulex europaeus* (Sigma-aldrich, USA–
453 l9006) and the antibodies anti-VWF (Santa Cruz Biotechnology, USA – sc14014), anti-
454 CD31 (Abcam, UK – ab28364), anti-ACE (Abcam, UK – ab85955), anti-CD62E
455 (Abcam - ab18981), anti-eNOS (Abcam, UK – ab87750) and anti-VE-cadherin
456 (Abcam, UK – ab205336) (Fig S1).

457

458 ***Plasmodium* synchronization and enrichment of parasitized erythrocytes**

459 To obtain mature forms of *P. berghei* ANKA, iRBCs were synchronized as described
460 previously (53). Succinctly, iRBCs were collected from infected mice exhibiting 10 to
461 20% parasitemia through cardiac puncture and transferred to RPMI 1640 culture
462 medium (Gibco-Thermo, USA) supplemented with 25% fetal bovine serum (FBS). The
463 iRBCs were subsequently maintained *in vitro* at 37°C for 14 h in an atmosphere

464 containing 5% CO_2, 85% N_2, and 10% O_2. The parasitized erythrocytes were then
465 enriched using a magnetic separation column (Miltenyi Biotec, USA) to generate cell
466 populations consisting of approximately 95% iRBCs, as assessed by thick blood smears.
467 *P. berghei* extract was obtained from iRBC subjected to several freeze-thawing cycles.
468

469 **Transwell assay with endothelial cells and peritoneal macrophages**

470 Sterile 13 mm diameter cover slip-knittel glass plates were placed in 24-well culture
471 plates. The coverslips were treated with 0.2% gelatin (gelatin from bovine skin - Sigma-
472 Aldrich) diluted in 1x PBS. PMLECS were seeded in the culture plate (7 x 10^4 cells /
473 well) in 400 µl of complete DMEM medium and 1x10^5 peritoneal macrophages (Mφ)
474 were seeded in the transwell membrane (6.5 mm membrane diameter, 0.4 µm
475 membrane pore, Corning, Costar 3470). After 24 hours, 2.5 x 10^6 mature forms of
476 iRBC or RBC were added over the Mφ and incubated for 24 hours. After this time, the
477 supernatant between Mφ and endothelial cells was collected for the quantification of
478 cytokines by ELISA. Subsequently, endothelial cells were stimulated with 1.75 x 10^6
479 iRBC for adhesion assay.
480

481 ***Plasmodium berghei* ANKA adhesion assay under static conditions**

482 DBA/2-PMLEC were plated in Lab-Tek slides "chamber slide" permanox of 8 wells
483 (3x10^4 cells/well) (Thermo Fisher Scientific - 177 455). Afterwards, the stimuli with
484 TNF-α (50ng/ml) are added and kept for 24, 48 or 72 hours. After stimulation,
485 synchronized PbA-iRBC were added for 1 hour in culture at a ratio of 25 iRBC/
486 PMLEC at 37 and 5% CO_2. After the incubation period, the culture medium was
487 removed and detached from the chamber slides, washed, fixed with methanol, stained
488 with Giemsa and then observed under an optical microscope immersion (magnification

489 1000 times). The counting pattern used was the observation of the number of adhered
490 parasites at 100 DBA/2-PMLEC and expressed as a percentage.
491

492 **Parasite adhesion assay in flow conditions**

493 PMLEC between 3rd and 5th passage was seeded ($8x10^4$/well) in 2-wells permanox
494 chamber slides labteck (Thermo Scientific, Nunc). The cells were incubated at 37 ° C
495 and 5% CO^2 for 24 hours. After this time, TNF might have been added for 24 hours or
496 not (control). In sequence, the stimulus was removed and mature forms of EP-PbA (25
497 per cell) in DMEM supplemented with 20% FBS were added and allowed to interact
498 with the endothelial cells for 1 hour at 37°C in 5% CO_2.
499 Subsequently, the wells were detached from the polystyrene slides and the slides were
500 added to the flow system composed of a chamber (Cell Adhesion Flow chamber,
501 Immunetics) which kept the slide adhered through the formation of a vacuum (coupled
502 by a vacuum pump), a syringe pump (insight Inc.), an inverted microscope (Zeiss Vert.
503 A1) connected to a camera (Axio Cam ERc 5s Zeiss) and to a computer with an image
504 capture system (program Zen 2011, AxioVision Rel 4.8.2 SP2).
505 The chamber was initially filled with DMEM medium, then an initial photo with the
506 parasites adhered to the CEPP-DBA/2 was taken, after, a medium continuous stream
507 was run through the chamber and maintained at 2 ml/hour with a pump syringe (Insight
508 Inc). Five images, every 3 minutes, of each well were captured, maintaining the same
509 field as the initial image, to determine the erythrocyte binding efficiency.
510 Image processing and analysis were performed by ImageJ (Version 1.46r). The images
511 were opened individually in ImageJ and analyzed through the "cell counter" plugin,
512 where all EP-PbA images were selected on each image. After counting all the images,
513 the total of EP-PbA that remained in the final image (15 minutes) was recorded. The

514 experiment was repeated with two independent cultures, each with two technical
515 replicates. Image processing and analysis was done in Image J.
516

517 **Treatment with dexamethasone**

518 80mg/kg of dexamethasone (Decadronal, ache) was inject intraperitoneally (ip) on
519 days 5 and 6 after infection 80 mg/kg, according to previously described [26].
520

521 **Lung permeability and edema**

522 To investigate lung permeability, non-infected or PbA-infected mice (dexamethasone-
523 treated or not), on the 7th dpi, were injected intravenously with 0.2mL of 1% Evans Blue
524 (Sigma). The mice were euthanized 45 minutes later, and the lungs were weighed
525 immediately and placed in 2mL of formamide (Merck) for 48 hours at 37∘C [12]. The
526 absorbance of the formamide was then measured at 620 nm and 740 nm. The amount of
527 Evans Blue staining per gram of lung tissue was calculated from a standard curve.
528

529 **Measure of primary microvascular lung endothelial cells permeability.**

530 The increased lung vascular permeability was analysed in DBA/2-PMLEC plated on
531 inserts of permeable membranes with 0.4µM pores (Transwell Corning), pre-treated
532 with gelatin and coupled in 24-well polystyrene plates at a concentration of 2.2×10^4
533 cells per insert and maintained in DMEM culture at 37°C, as previously described (15).
534 After 96 hours, until the cells reach confluency, the extract was applied for 1h after
535 incubation with dexamethasone (500 ng/ml during 24 h) or solely with 20% FBS
536 supplemented DMEM culture medium. Subsequently, the culture medium was replaced
537 by Hank's balanced salt solution and in the upper compartment of each insert, in contact
538 with the cells; 200µl of Evans Blue was incubated at 2mg/mL concentration at 37°C.

539 After 30 min, the liquid from the lower compartment was collected and analysed in a
540 spectrophotometer at 650 nm wavelength (NanoDrop 2000, Thermo Scientific). Finally,
541 the concentration of Evans Blue was determined from a standard curve (0.2mg/mL to
542 0.0031mg/mL) as previously known.
543

544 **Actin Microfilaments Identification by Immunofluorescent and Morphometric**
545 **Analysis of the Opening of Interendothelial Junctions.**

546 In order to analyse the area of interendothelial junctions, PMLEC were plated in 24 well
547 plates (7×10^4 cells/well), adhered to gelatin on glass coverslips, and maintained at 37°C
548 and 5% CO_2. The cells were stimulated with either iRBC or RBC for 1 h, after
549 incubation with dexamethasone (24 hours), or solely with DMEM culture medium,
550 supplemented with 20% FBS, in triplicate. Subsequently, the cells were fixed with 3.7%
551 formaldehyde, permeabilized with acetone at −20°C, and blocked with bovine serum
552 albumin solution (1% BSA). Actin was marked with Texas Red Phalloidin (T7471, Life
553 Technologies) by 20 minutes. The cell nuclei were marked with Hoechst (H33342, Life
554 Technologies). Each slide, with fully confluent cells, was chosen randomly and ten to
555 twenty pictures were taken and scanned in a "zig-zag" way, from top to bottom. The
556 images were acquired in the fluorescence Axio Imager M2 microscope (Zeiss) using the
557 Axio Cam HRc (Zeiss) and the software Axio Vision, version 4.9.1.0. The total area of
558 OIJ was measured in each picture using the software ImageJ.
559

560 **TNF-blockage**

561 TNF was blocked in DBA-PMLEC using Mouse TNF Neutralizing (D2H4) Rabbit
562 mAb #11969 (Cell signaling®) in a concentration of 1 μg/ml for 24 hours in PMLEC.

563

564 **Soluble EPCR quantification**

565 Soluble endothelial protein C receptor (sEPCR) was measured with an ELISA kit
566 (Elabscience®, E-EL-M1073), according to the manufacturer's instructions.

567

568 **EPCR Western Blot**

569 Fresh frozen mice lung tissues collected on the 7th dpi were sonicated and homogenized
570 at 4°C, using the Radio-Immunoprecipitation Assay (RIPA) buffer composed of 50 mM
571 TrisHCl pH 8.0, 150 mM NaCl, 0.5% sodium deoxycholate, 0.2% sodium dodecyl
572 sulphate (SDS), 1 mM sodium orthovanadate, 1 mM NaF, and a protease inhibitor
573 tablet. The total protein concentration was determined using a SpectraMax® Plus 384
574 (Molecular Devices) spectrophotometer with a 562 nm filter using the Pierce ™ BCA
575 Protein Assay kit (Thermo Scientific) according to the manufacturer instructions. Then,
576 30 µg of protein from each sample was electrophoretically separated in 10%
577 polyacrylamide mini-gel (Bio-Rad) with SDS-PAGE at 100V for 2 hours, in a Mini-
578 PROTEAN® Tetra cell apparatus (Bio-Rad). The Kaleidoscope commercial standard
579 Precision Plus Protein (Bio-Rad), standard molecular weight, was used. Subsequently,
580 proteins separated on the gel were transferred to PVDF (Polyvinylidene Difluoride, 0.2
581 µm, Bio-Rad) membranes in transfer buffer (0.1 M glycine, 0.02 M Tris, 20% methanol
582 and MilliQ water) overnight at 4ºC in a wet transfer apparatus at 70mA constant voltage
583 (Bio-Rad). Detection of chemiluminescence immunochemical reaction was performed
584 on a ChemiDoc ™ XRS + Molecular Imager® (Bio-Rad) transilluminator with
585 ImageLab ™ program (Bio-Rad). Blocking of non-specific sites was carried out after
586 the transfer; (Tris-buffer-saline-Twin-20 buffer, 0.05 M TRIS, 0.1 M NaCl, pH 7.3 and
587 0.1% Twin-20, Synth), BSA 3% under a 2 h stirring at room temperature (RT). The

588 membrane was then incubated with the primary anti-EPCR antibody (# 151403, abcam)
589 1: 1,000 stirring overnight at 4°C. After washing in TBS-T, the membrane was
590 incubated with the peroxidase-conjugated rabbit anti-rabbit IgG (HRP) secondary
591 antibody (# AP307P, Millipore) at 1: 6,000 concentration in TBS-T for 1 hour (RT).
592 Bands were detected by the chemiluminescence method Clarity Western ECL (Bio-Rad)
593 for EPCR and the housekeeping protein β-actin (mouse IgG # NB600-501, Novus, at
594 the 1: 40,000) and finally, densiometrically measured by ImageJ 1.6.0 software.

595

596 **Bronchoalveolar lavage and VEGF quantification**

597 On the 7th dpi, infected mice (not-treated or treated with dexamethasone) were
598 anesthetized, and for bronchoalveolar lavage (BAL) collection, the trachea was
599 cannulated, and lungs were washed once with 1.0 ml of PBS 1X. An ELISA kit
600 (R&DSystems, USA) was used to quantify VEGF levels in BAL and in culture
601 supernatant according to the manufacturer instructions.

602

603 **Transfection of EPCR siRNA**

604 To transfect EPCR to interference RNA assay, Lipofectamine® RNAiMAX Reagent
605 (Invitrogen, by life technologies) and a poll of 3 different oligonucleotides silencer
606 select pre-designed and validated siRNA (Ambion, by life technologies) were used
607 according to the manufacturing protocol. Also, a Silencer Select Negative Control
608 (Ambion 4390843) and a silencer select GAPDH positive control (Ambion 4390849)
609 were employed.

610 siRNA1: forward: 5' CAACCGGACUCGGUAUGAATT 3;

611 reverse: 5'UUCAUACCGAGUCCGGUUGta3'

siRNA2: forward: 5'ACGCAAAACAUGAAAGGGATT 3';

reverse: 5'UCCCUUUCAUGUUUUGCGUGG 3'

siRNA3:forward: 5' CGCCCUUUGUAACUCCGAUTT 3';

reverse: 5'AUCGGAGUUACAAAGGGCGCA3'

Statistical Analysis

The statistical analyses were performed using the GraphPad Prism® 5.0 software for analysis and graphing. The data were analysed for normality by Kolmogorov-Smirnov test or Shapiro-Wilk normality test and the variance with Bartlett test. Non-parametric variables for two groups were compared by using Mann-Whitney test. For analysis of three groups, we used Kruskal-Wallis test followed Dunn post-test. In order to compare parametrical variables for two groups, T-test was employed and for three or more groups, One-way ANOVA followed by Bonferroni post-test were used. For the survival curves, Log-rank and Gehan-Breslow Wilcoxon tests were applied. The differences between the groups were considered significant when $p \leq 0.05$ (5%). To establish a cut-off from data, ROC curves were generated by using the results of the control group obtained in MedCalc version 8.2.1.0.

Acknowledgments

The authors thank Patricia Mendonça da Silva Amorim and Erika Paula Machado Peixoto for their technical support.

REFERENCES

1. Craig AG, Khairul MFM, Patil PR. Cytoadherence and severe malaria. Malays J Med Sci. 2012;19: 5–18. Available:

637 http://www.pubmedcentral.nih.gov/articlerender.fcgi?artid=3431742&tool=pmce
638 ntrez&rendertype=abstract

639 2. Beeson JG, Brown G V. Pathogenesis of Plasmodium falciparum malaria: the
640 roles of parasite adhesion and antigenic variation. Cell Mol Life Sci. 2002;59:
641 258–71. doi:1420-682X/02/020258-14

642 3. Miller LH, Baruch DI, Marsh K, Doumbo OK. The pathogenic basis of malaria.
643 Nature. 2002;415: 673–9. doi:10.1038/415673a

644 4. Greenwood BM, Fidock DA, Kyle DE, Kappe SHI, Alonso PL, Collins FH, et al.
645 Malaria: progress, perils, and prospects for eradication. J Clin Invest. 2008;118:
646 1266–76. doi:10.1172/JCI33996

647 5. Pouvelle B, Buffet P a, Lépolard C, Scherf a, Gysin J. Cytoadhesion of
648 Plasmodium falciparum ring-stage-infected erythrocytes. Nat Med. 2000;6:
649 1264–8. doi:10.1038/81374

650 6. Rénia L, Wu Howland S, Claser C, Charlotte Gruner A, Suwanarusk R, Hui Teo
651 T, et al. Cerebral malaria: mysteries at the blood-brain barrier. Virulence. 2012;3:
652 193–201. doi:10.4161/viru.19013

653 7. Grommes J, Soehnlein O. Contribution of neutrophils to acute lung injury. Mol
654 Med. 2011;17: 293–307. doi:10.2119/molmed.2010.00138

655 8. Bhatia M, Zemans RL, Jeyaseelan S. Role of chemokines in the pathogenesis of
656 acute lung injury. Am J Respir Cell Mol Biol. 2012;46: 566–72.
657 doi:10.1165/rcmb.2011-0392TR

658 9. Matute-Bello G, Martin TR. Science review: apoptosis in acute lung injury. Crit
659 Care. 2003;7: 355–8. doi:10.1186/cc1861

660 10. Van den Steen PE, Deroost K, Deckers J, Van Herck E, Struyf S, Opdenakker G.
661 Pathogenesis of malaria-associated acute respiratory distress syndrome. Trends
662 Parasitol. Elsevier Ltd; 2013;29: 346–358. doi:10.1016/j.pt.2013.04.006

663 11. Lovegrove FE, Gharib S a, Peña-Castillo L, Patel SN, Ruzinski JT, Hughes TR,
664 et al. Parasite burden and CD36-mediated sequestration are determinants of acute
665 lung injury in an experimental malaria model. PLoS Pathog. 2008;4: e1000068.
666 doi:10.1371/journal.ppat.1000068

667 12. Ortolan LS, Sercundes MK, Barboza R, Debone D, Murillo O, Hagen SCF, et al.
668 Predictive criteria to study the pathogenesis of malaria-associated ALI/ARDS in
669 mice. Mediators Inflamm. 2014;2014: 872464. doi:10.1155/2014/872464

670 13. Epiphanio S, Campos MG, Pamplona A, Carapau D, Pena AC, Ataíde R, et al.
671 VEGF promotes malaria-associated acute lung injury in mice. PLoS Pathog.
672 2010;6: e1000916. doi:10.1371/journal.ppat.1000916

673 14. Sercundes MK, Ortolan LS, Debone D, Soeiro-Pereira P V., Gomes E, Aitken
674 EH, et al. Targeting neutrophils to Prevent Malaria-Associated Acute Lung
675 Injury/Acute respiratory Distress Syndrome in Mice. PLOS Pathog. 2016;12:
676 e1006054. doi:10.1371/journal.ppat.1006054

677 15. Pereira MLM, Ortolan LS, Sercundes MK, Debone D, Murillo O, Lima FA, et al.
678 Association of Heme Oxygenase 1 with Lung Protection in Malaria-Associated
679 ALI/ARDS. Mediators Inflamm. 2016;2016. doi:10.1155/2016/4158698

680 16. El-Assaad F, Wheway J, Mitchell AJ, Lou J, Hunt NH, Combes V, et al.
681 Cytoadherence of Plasmodium berghei-infected red blood cells to murine brain
682 and lung microvascular endothelial cells in vitro. Infect Immun. 2013;81: 3984–
683 3991. doi:10.1128/IAI.00428-13

684 17. Cunningham DA, Lin J, Brugat T, Jarra W, Tumwine I, Kushinga G, et al.
685 ICAM-1 is a key receptor mediating cytoadherence and pathology in the
686 Plasmodium chabaudi malaria model. Malar J. 2017;16: 185.
687 doi:10.1186/s12936-017-1834-8

688 18. Aird WC, Mosnier LO, Fairhurst RM. Plasmodium falciparum picks (on) EPCR.
689 Blood. 2014;123: 163–167. doi:10.1182/blood-2013-09-521005

690 19. Turner L, Lavstsen T, Berger SS, Wang CW, Petersen JE V, Avril M, et al.
691 Severe malaria is associated with parasite binding to endothelial protein C
692 receptor. Nature. Nature Publishing Group; 2013;498: 502–5.
693 doi:10.1038/nature12216

694 20. Rao LVM, Esmon CT, Pendurthi UR. Endothelial cell protein C receptor: A
695 multiliganded and multifunctional receptor. Blood. 2014. doi:10.1182/blood-
696 2014-05-578328

697 21. Shabani E, Opoka RO, Bangirana P, Park GS, Vercellotti GM, Guan W, et al.
698 The endothelial protein C receptor rs867186-GG genotype is associated with
699 increased soluble EPCR and could mediate protection against severe malaria. Nat
700 Publ Gr. 2016; doi:10.1038/srep27084

701 22. Mosnier LO, Lavstsen T. The role of EPCR in the pathogenesis of severe
702 malaria. Thromb Res. 2016; doi:10.1016/S0049-3848(16)30364-4

703 23. Turner L, Lavstsen T, Berger SS, Wang CW, Petersen JE V, Avril M, et al.
704 Severe malaria is associated with parasite binding to endothelial protein C
705 receptor. 2013; doi:10.1038/nature12216

706 24. Azasi Y, Lindergard G, Ghumra A, Mu J, Miller LH, Rowe JA. Infected
707 erythrocytes expressing DC13 PfEMP1 differ from recombinant proteins in
708 EPCR-binding function. Proc Natl Acad Sci. 2018; 201712879.
709 doi:10.1073/pnas.1712879115

710 25. Aitken EH, Negri EM, Barboza R, Lima MRI, Alvarez JM, Marinho CRF, et al.
711 Ultrastructure of the lung in a murine model of malaria-associated acute lung
712 injury/acute respiratory distress syndrome. Malar J. 2014;13: 230.
713 doi:10.1186/1475-2875-13-230

714 26. Van den Steen PE, Geurts N, Deroost K, Van Aelst I, Verhenne S, Heremans H,
715 et al. Immunopathology and dexamethasone therapy in a new model for malaria-
716 associated acute respiratory distress syndrome. Am J Respir Crit Care Med.
717 2010;181: 957–68. doi:10.1164/rccm.200905-0786OC

718 27. Pino P, Vouldoukis I, Kolb JP, Mahmoudi N, Desportes-Livage I, Bricaire F, et

al. Plasmodium falciparum--infected erythrocyte adhesion induces caspase activation and apoptosis in human endothelial cells. J Infect Dis. 2003;187: 1283–90. doi:10.1086/373992

28. de Souza JB, Riley EM. Cerebral malaria: the contribution of studies in animal models to our understanding of immunopathogenesis. Microbes Infect. 2002;4: 291–300. Available: http://www.ncbi.nlm.nih.gov/pubmed/11909739

29. Braks J, Aime E, Spaccapelo R, Klop O, Janse CJ, Franke-Fayard B. Bioluminescence imaging of P. berghei schizont sequestration in rodents. Methods Mol Biol. 2013;923: 353–368. doi:10.1007/978-1-62703-026-7-25

30. Franke-Fayard B, Fonager J, Braks A, Khan SM, Janse CJ. Sequestration and tissue accumulation of human malaria parasites: Can we learn anything from rodent models of malaria? PLoS Pathog. 2010;6: e1001032. doi:10.1371/journal.ppat.1001032

31. Jaramillo M, Godbout M, Olivier M. Hemozoin induces macrophage chemokine expression through oxidative stress-dependent and -independent mechanisms. J Immunol. 2005;174: 475–84. Available: http://www.ncbi.nlm.nih.gov/pubmed/15611273

32. Shio MT, Kassa FA, Bellemare MJ, Olivier M. Innate inflammatory response to the malarial pigment hemozoin. Microbes Infect. 2010;12: 889–899. doi:10.1016/j.micinf.2010.07.001

33. Coban C, Ishii KJ, Kawai T, Hemmi H, Sato S, Uematsu S, et al. Toll-like receptor 9 mediates innate immune activation by the malaria pigment hemozoin. J Exp Med. 2005;201: 19–25. doi:10.1084/jem.20041836

34. Parroche P, Lauw FN, Goutagny N, Latz E, Monks BG, Visintin A, et al. Malaria hemozoin is immunologically inert but radically enhances innate responses by presenting malaria DNA to Toll-like receptor 9. Proc Natl Acad Sci U S A. 2007;104: 1919–24. doi:10.1073/pnas.0608745104

35. De las Salas B, Segura C, Pabón A, Lopes SCP, Costa FTM, Blair S. Adherence to human lung microvascular endothelial cells (HMVEC-L) of Plasmodium vivax isolates from Colombia. Malar J. 2013;12: 347. doi:10.1186/1475-2875-12-347

36. El-Assaad F, Wheway J, Mitchell AJ, Lou J, Hunt NH, Combes V, et al. Cytoadherence of plasmodium berghei-infected red blood cells to murine brain and lung microvascular endothelial cells in vitro. Infect Immun. 2013;81: 3984–3991. doi:10.1128/IAI.00428-13

37. Maknitikul S, Luplertlop N, Grau GER, Ampawong S. Dysregulation of pulmonary endothelial protein C receptor and thrombomodulin in severe falciparum malaria-associated ARDS relevant to hemozoin. PLoS One. 2017;12: e0181674. doi:10.1371/journal.pone.0181674

38. Bhatia M, Moochhala S. Role of inflammatory mediators in the pathophysiology of acute respiratory distress syndrome. J Pathol. 2004;202: 145–56. doi:10.1002/path.1491

39. Cayrol C, Girard JP. Interleukin-33 (IL-33): A nuclear cytokine from the IL-1

761 family. Immunol Rev. 2018;281: 154–168. doi:10.1111/imr.12619

762 40. Ampawong S, Chaisri U, Viriyavejakul P, Prapansilp P, Grau GE, Turner GDH,
763 et al. A potential role for interleukin-33 and γ-epithelium sodium channel in the
764 pathogenesis of human malaria associated lung injury. Malar J. BioMed Central;
765 2015;14: 1–15. doi:10.1186/s12936-015-0922-x

766 41. Palomo J, Reverchon F, Piotet J, Besnard AG, Couturier-Maillard A, Maillet I, et
767 al. Critical role of IL-33 receptor ST2 in experimental cerebral malaria
768 development. Eur J Immunol. 2015;45: 1354–1365. doi:10.1002/eji.201445206

769 42. Reverchon F, Mortaud S, Sivoyon M, Maillet I, Laugeray A, Palomo J, et al. IL-
770 33 receptor ST2 regulates the cognitive impairments associated with
771 experimental cerebral malaria. PLoS Pathog. 2017;13: 1–25.
772 doi:10.1371/journal.ppat.1006322

773 43. Besnard AG, Guabiraba R, Niedbala W, Palomo J, Reverchon F, Shaw TN, et al.
774 IL-33-Mediated Protection against Experimental Cerebral Malaria Is Linked to
775 Induction of Type 2 Innate Lymphoid Cells, M2 Macrophages and Regulatory T
776 Cells. PLoS Pathog. 2015;11: 1–21. doi:10.1371/journal.ppat.1004607

777 44. Randeep S. Jawa, Sergio Anillo, Kristin Huntoon, Heinz Baumann MK. Analytic
778 Review: Interleukin-6 in Surgery, Trauma, and Critical Care: Part I: Basic
779 Science. J Intensive Care Med. 2011;26: 3–12.
780 doi:https://doi.org/10.1177/0885066610395678

781 45. Park WY, Goodman RB, Steinberg KP, Ruzinski JT, Ii FR, Park DR, et al.
782 Cytokine Balance in the Lungs of Patients with Acute Respiratory Distress
783 Syndrome. 2001; 1896–1903. doi:10.1164/rccm2104013

784 46. Takala A, Jousela I, Takkunen O, Kautiainen H, Jansson S-E, Orpana A, et al. A
785 prospective study of inflammation markers in patients at risk of indirect acute
786 lung injury. Shock. 2002;17: 252–7. doi:10.1097/00024382-200204000-00002

787 47. Wilson MR, Wakabayashi K, Bertok S, Oakley CM, Patel B V., O'Dea KP, et al.
788 Inhibition of TNF receptor p55 by a domain antibody attenuates the initial phase
789 of acid-induced lung injury in mice. Front Immunol. 2017;8: 1–12.
790 doi:10.3389/fimmu.2017.00128

791 48. Wilson MR, Goddard ME, O'Dea KP, Choudhury S, Takata M. Differential roles
792 of p55 and p75 tumor necrosis factor receptors on stretch-induced pulmonary
793 edema in mice. Am J Physiol Cell Mol Physiol. 2007;293: L60–L68.
794 doi:10.1152/ajplung.00284.2006

795 49. Proudfoot A, Bayliffe A, O'Kane CM, Wright T, Serone A, Bareille PJ, et al.
796 Novel anti-tumour necrosis factor receptor-1 (TNFR1) domain antibody prevents
797 pulmonary inflammation in experimental acute lung injury. Thorax. 2018;1:
798 thoraxjnl-2017-210305. doi:10.1136/thoraxjnl-2017-210305

799 50. Lin JW, Sodenkamp J, Cunningham D, Deroost K, Tshitenge TC, McLaughlin S,
800 et al. Signatures of malaria-associated pathology revealed by high-resolution
801 whole-blood transcriptomics in a rodent model of malaria. Sci Rep. Nature
802 Publishing Group; 2017;7: 1–13. doi:10.1038/srep41722

803 51. Livak KJ, Schmittgen TD. Analysis of relative gene expression data using real-
804 time quantitative PCR and the 2(-Delta Delta C(T)) Method. Methods. 2001;25:
805 402–8. doi:10.1006/meth.2001.1262

806 52. Chen SF, Fei X, Li SH. A new simple method for isolation of microvascular
807 endothelial cells avoiding both chemical and mechanical injuries. Microvasc Res.
808 1995;50: 119–28. doi:10.1006/mvre.1995.1044

809 53. Trager W, Jensen JB. Human malaria parasites in continuous culture. Science
810 (80-). 1976;193: 673–675.

811

812

813 ## Figure Captions

814 **Fig 1. ARDS-developing mice showing higher load pulmonary parasite than HP-**
815 **developing mice.** (A) Infected mice had luminescence signal in the peripheral blood
816 and tissues and (B and C) perfused infected mice showing luciferase/luciferin signal on
817 the 7th day after infection. (B and C) The luminescence was more concentrated in lungs
818 and spleen. Images taken in IVIS® Spectrum *in vivo* imaging system [Kruskal-Wallis
819 test and post-test Dunn's, n= 3. Bars represent mean ± SEM (*, p<0,05)]. (D) rRNA
820 gene expression of *P. berghe*i ANKA (subunit 18s) in lung tissue of euthanized mice on
821 the 7th day after infection, using $2^{-\Delta\Delta CT}$ method. ARDS-developing mice (n= 15) have
822 more *P. berghei* mRNA than HP mice (n= 12 HP); (E-G) Hemozoin quantification in
823 polarized light [(magnification: 400x, scale bar: 20µm n=3 mice/group, (10 images for
824 each tissue) bars represent mean ± SEM (*, p<0,05 Student's T-test)]. (H) Lung
825 histological analyses showing iRBC in close contact to endothelial cells in a mouse that
826 died by ARDS (magnification: 630x, scale bar: 10 µm). HP: hyperparasitemia; ARDS:
827 acute acute respiratory distress syndrome; iRBC: infected red blood cells. Infection of
828 DBA/2 mice with *P. berghei* Luciferase (PbA-luciferase). Lu: lung; Sp: spleen; Ki:
829 kidney; Li: liver; Br: brain; He: heart.

830 **Fig 2. TNF increases *Plasmodium berghei* adherence in ARDS experimental model.**
831 (A) ARDS-developing mice (n= 10) have more TNF in serum compared to HP (n= 8)
832 and NI mice (n= 6 NI); (B) PMLEC stimulated with iRBC secrets more TNF compared
833 to NS cells within 24 hours (ELISA, n= 4/ group). PMLEC stimulated with TNF have
834 more adhesion of iRBC compared to not stimulated cells (NS) in (C) 24 hours (n= 4 NS,
835 4iRBC), (D) 48 hours (n= 7 NS, 6 TNF) and (E) 72 hours in static conditions and (n= 7
836 NS, 6 TNF) (F-H) in flow conditions (n= 2 NS; 4 TNF). (I-K) A transwell assay with
837 peritoneal macrophages (Mφ) in indirect contact with endothelial cells shows that Mφ
838 stimulated with iRBC for 24 hours produce a large quantity of (J) TNF compared to
839 non-stimulated cells. (K) Moreover, PMLEC, in indirect contact with Mφ with
840 previously stimulus with iRBC, showed more capacity of iRBC adherence then cells
841 without previously contact with Mφ (J-K: n= 3-4/group). (L) TNF neutralizing reduced
842 iRBC adherence in PMLEC (n= 8/group). Bars represent mean ± SEM, Graphics A, J.
843 K and L: Nonparametric ANOVA, Kruskal-Wallis test, Post Test Dunns. Graphics B, C,
844 D, E and H: Mann-Whitney T test (*p<0,05; ** p<0,01; *** p<0,001). ARDS: acute
845 respiratory distress syndrome; HP: hyperparasitemia; PMLEC: primary culture of
846 microvascular lung endothelial cells from DBA/2 mice; Mφ: peritoneal macrophage;
847 NS: non-stimulated cells; RBC: red blood cell; iRBC: infected red blood cells.

848 **Fig 3. EPCR acts directly in *P. berghei* cytoadherence.** (A) ARDS-developing mice
849 have more EPCR mRNA expression in lungs (n= 17 ARDS, 11 HP), (B) more soluble
850 EPCR (sEPCR) in sera (n= 4/group), and (C) more EPCR protein in lungs compared to
851 HP mice (n= 6 ARDS, 5 HP). PMLEC stimulated with TNF show upregulation in
852 EPCR expression compared to non-stimulated cells (NS) or cells stimulated with iRBC
853 in (D) 24 hours (n= 4 NS, 6 iRBC, 6 TNF), (E) 48 hours (n= 5 NS, 6 iRBC, 6 TNF) and
854 (F) 72 hours after treatment (n=4 NS, 5 iRBC, 6 TNF). (G) EPCR knockdown reduced

855 EPCR mRNA expression in PMLEC (n= 6/group) and (H) reduced iRBC adherence in
856 PMLEC compared to TNF stimulated cells (n= 7/ group). Bars represent mean ± SEM.
857 Graphics A and B: Mann-Whitney T test; Graphics D-H: Nonparametric ANOVA,
858 Kruskal-Wallis test, Post Test Dunns (*p<0,05; **p<0,01; ***p<0,001). ARDS: acute
859 respiratory distress syndrome; HP: hyperparasitemia; PMLEC: primary culture of
860 microvascular lung endothelial cells from DBA/2 mice; NS: non-stimulated cells; RBC:
861 red blood cell; iRBC: infected red blood cells. Red dashed lines: non-infected mice
862 mean.

863 **Fig 4. Dexamethasone reduces TNF and EPCR, protecting mice lungs and PMLEC**
864 **from increased vascular permeability.** (A) TNF mRNA expression is reduced in
865 Dexamethasone-treated mice (n= 5/group). (B) EPCR mRNA expression in lungs (n=
866 9/group) and (C) sEPCR concentration in serum (n= 4 Infected, 8 Infected+Dexa) and
867 in (D) BAL is down regulated in Infected+Dexa (n= 4) compared to infected-not-treated
868 mice (n= 5). (E) VEGF concentration is also decreased in Infected+Dexa mice (n=
869 5/group). (F-G) Infected+Dexa mice have less Evans blue accumulated in lungs
870 compared to NI or infected mice (after perfusion) (n=4/group) and (H) reduced lung
871 weight (n= 4/group). (I-J) Actin microfilaments staining in PMLEC (grey) and nuclei
872 stained with Hoechst (blue) showing that endothelial cells stimulated with
873 dexamethasone have less opening in the interendothelial junctions (indicated by yellow
874 arrows) compared to non-treated cells. (K) PMLEC stimulated with iRBC and treated
875 with dexamethasone (n=12) have less Evans blue flow-through compared to non-treated
876 cells (n= 11) in a transwell assay and (L) decreased VEGF concentration. iRBC:
877 infected red blood cells; Infected+Dexa: mice infected with *P. berghei* ANKA and
878 treated with dexamethasone (n= 4/group); BAL: Bronchoalveolar lavage; iRBC:
879 infected red blood cells; Red dashed lines: non-infected mice mean. Bars represent

880 mean ± SEM (*, p<0,05; *** p<0,001) (A-D; F-G; J-K Mann-Whitney test; I and L
881 kruskal-Wallys test).

882 **Fig 5. Dexamethasone protects mice from ARDS but not from malaria infection.**
883 (A) Respiratory frequency, (B) tidal volume and (C) enhanced respiratory pause
884 improved in Infected+Dexa mice compared to those infected-control. (D) Parasitemia of
885 Infected+Dexa mice is increased but (E) they survive more compared to infected-not-
886 treated mice (A-E: n= 9 infected, 8 Infected+Dexa). Representative image of
887 histological analyze of (F) infected mice and (G) Infected+Dexa mice (Scale bar: 50
888 µm). Infected+Dexa: mice infected with *P. berghei* ANKA and treated with
889 dexamethasone. Red dashed lines: non-infected mice mean. Bars represent mean ±
890 SEM. Graphics A-D: Mann-Whitney T test. (*p<0,05; ** p<0,01).

891 **Fig 6. Schematic representation of ARDS development involving adhesion of iRBC**
892 **to EPCR.** *Plasmodium berghei* ANKA infected red blood cells (iRBC) induce TNF
893 release by endothelial cells. The stimulus with TNF up-regulate EPCR expression in
894 PMLEC, which increases the adhesion of iRBC in PMLEC through EPCR pathway.
895 The adhesion of iRBC in PMLEC lead to the increase of gap formations in the
896 interendothelial junction, increase in vascular permeability with infiltration of
897 inflammatory cells, red blood cells and edema. Activated alveolar macrophages also
898 produce TNF, which contribute to the activation of endothelial cells, recruitment of
899 neutrophils and alveolar damage. Mice treatment with dexamethasone decrease
900 inflammatory cytokines release, including TNF and consequently downregulate EPCR
901 expression in PMLEC; the dexamethasone also decreases VEFG released by endothelial
902 cells, protecting mice from gap formations, vascular permeability, inflammatory cells
903 infiltration and alveolar damage. PMLEC: primary culture of microvascular lung
904 endothelial cells from DBA/2 mice.

905

906 ## Supporting information

907 **S1 Fig. Primary microvascular lung endothelial cell characterization.** PMLEC were
908 stained by immunofluorescence with Lectin from *Ulex europaeus,* and anti- vWF,
909 CD31, ACE, CD62E, eNOS and Ve-cadherin antibodies. Nuclei stained with Hoechst
910 (blue). PMLEC: primary culture of microvascular lung endothelial cells from DBA/2
911 mice. (scale bar: 50 μm).

912 **S2 Fig. ARDS-developing mice show more ICAM-1 and VCAM expression in**
913 **lungs compared to HP-developing or non-infected mice. (A)** Immunohistochemistry
914 of ICAM-1 and VCAM in lungs of NI, ARDS-developing and HP-developing mice on
915 the 7th day post infection (scale bar: 100 μm). There was a decrease in (B) ICAM-1 area
916 in HP-developing mice compared to ARDS-developing and NI mice (n= 11 NI, 39
917 ARDS, 38 HP) and an increase in (C) VCAM area of ARDS-developing mice compared
918 to NI mice (n= 12 NI, 53 ARDS, 33 HP). (D-I) There was an intensification of ICAM-1
919 and VCAM mRNA expressions in PMLEC stimulated with TNF for 24, 48 and 72
920 hours compared to NS or cells stimulated with iRBC, measured by qRT-PCR. (D-I: n=
921 9 NS, 6 iRBC, 6 TNF). Bars represent mean ± SEM; Kruskal-Wallis test, *$p<0.05$; **
922 $p<0.01$; *** $p<0.001$. ARDS: acute respiratory distress syndrome; HP:
923 hyperparasitemia; NI: non-infected mice; NS: non-stimulated cells; iRBC: infected red
924 blood cells; PMLEC: primary culture of microvascular lung endothelial cells from
925 DBA/2 mice.

926 **S3 Fig. Dexamethasone reduced inflammation, but not decreased ICAM-1**
927 **expression in *P. berghei*-infected mice.** Infected+Dexa mice show a decrease in serum
928 levels of (A) IL-6 and (B) IL-33 compared to infected and non-treated mice (A-B: n= 5

929 Infected, 5 Infected+Dexa). (C) There was no difference in ICAM-1 mRNA expression
930 between Infected+Dexa and infected and non-treated mice lungs and there was a
931 decrease in VCAM mRNA expression in lungs of Infected+Dexa compared to infected-
932 non-treated mice (C-D: n= 9 Infected, 8 Infected+Dexa). Samples collected on the 7th
933 day post infection. Infected+Dexa: mice infected with *P. berghei* ANKA and treated
934 with dexamethasone. Red dashed lines: non-infected mice. Bars represent mean ± SEM.
935 Mann-Whitney T test (** $p<0,01$).

936

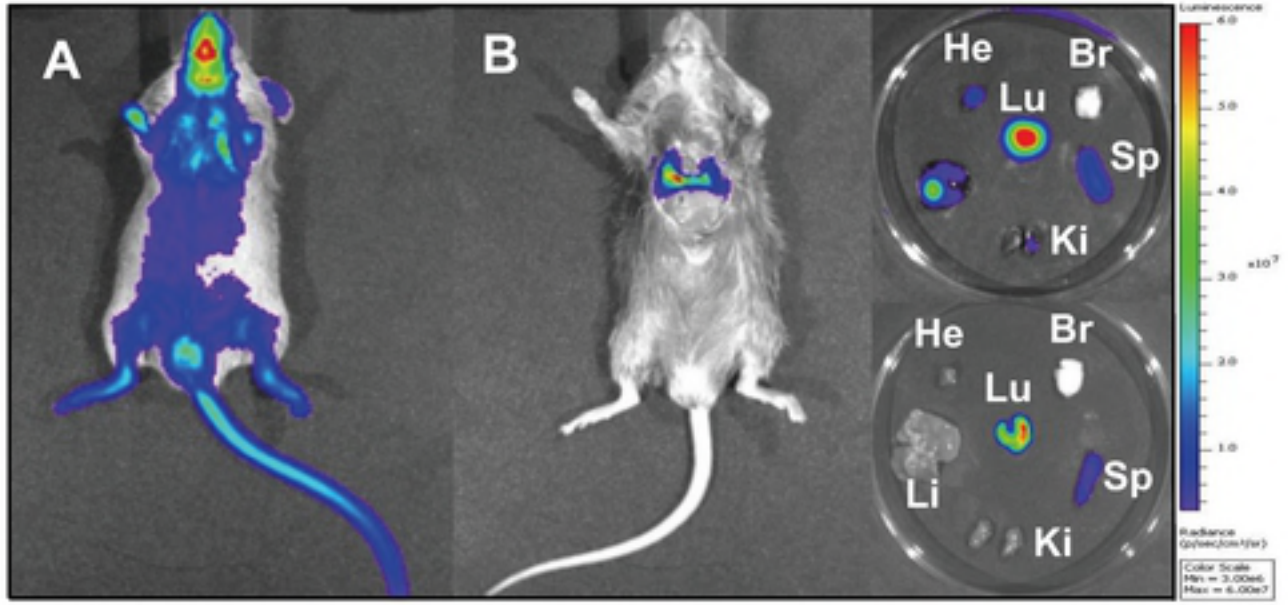
A
B
He
Br
Lu
Sp
Ki
He
Br
Lu
Li
Sp
Ki

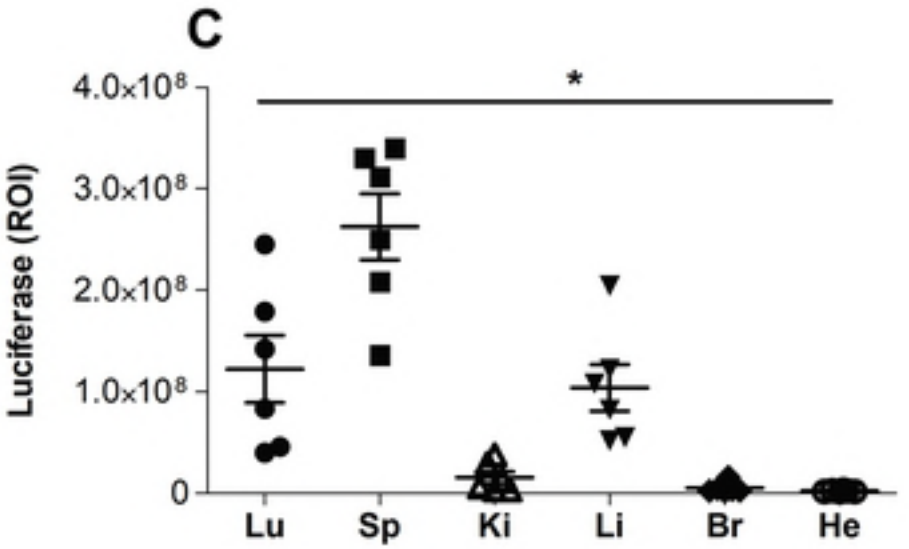
C
*
Luciferase (ROI)
4.0×10^8
3.0×10^8
2.0×10^8
1.0×10^8
0
Lu
Sp
Ki
Li
Br
He

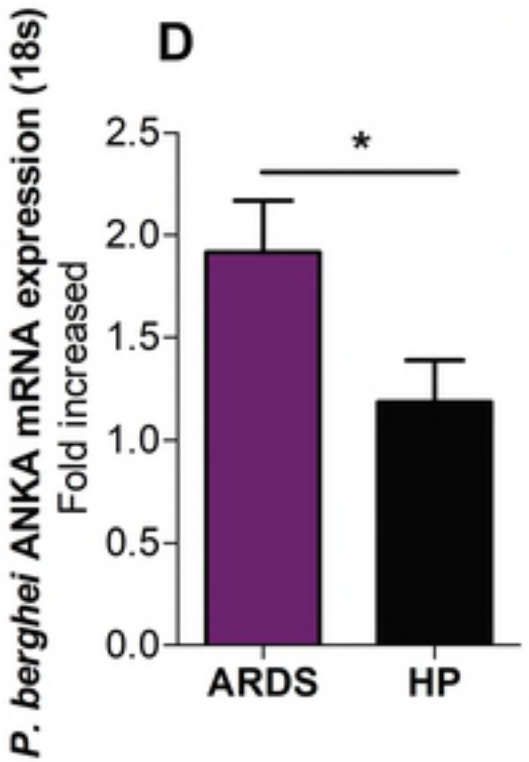
D
*
P. berghei ANKA mRNA expression (18s)
Fold increased
2.5
2.0
1.5
1.0
0.5
0.0
ARDS
HP

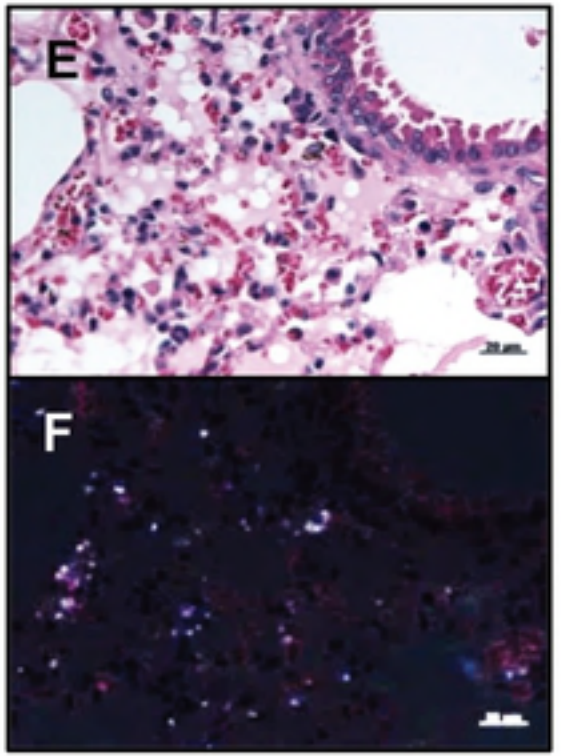
E
F

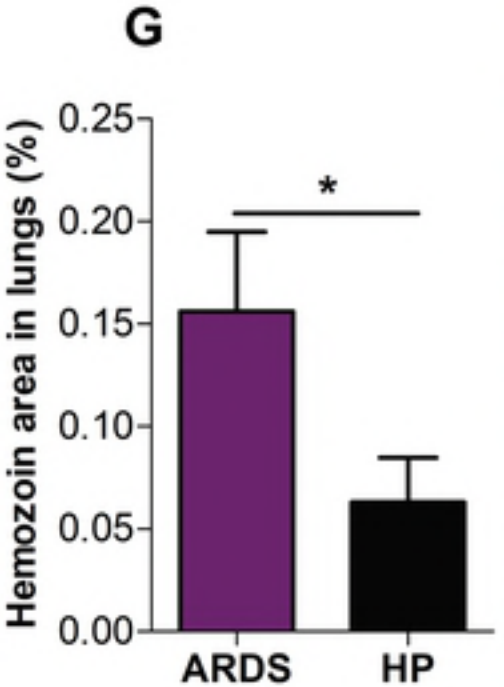
G
*
Hemozoin area in lungs (%)
0.25
0.20
0.15
0.10
0.05
0.00
ARDS
HP

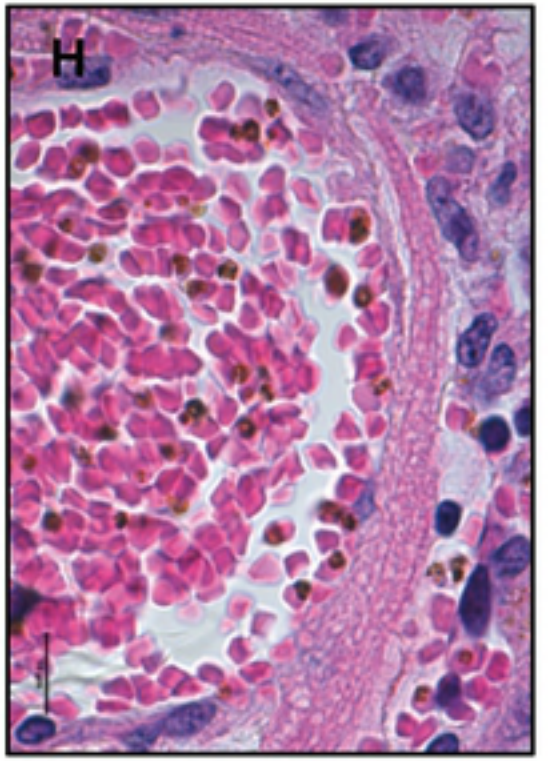
H

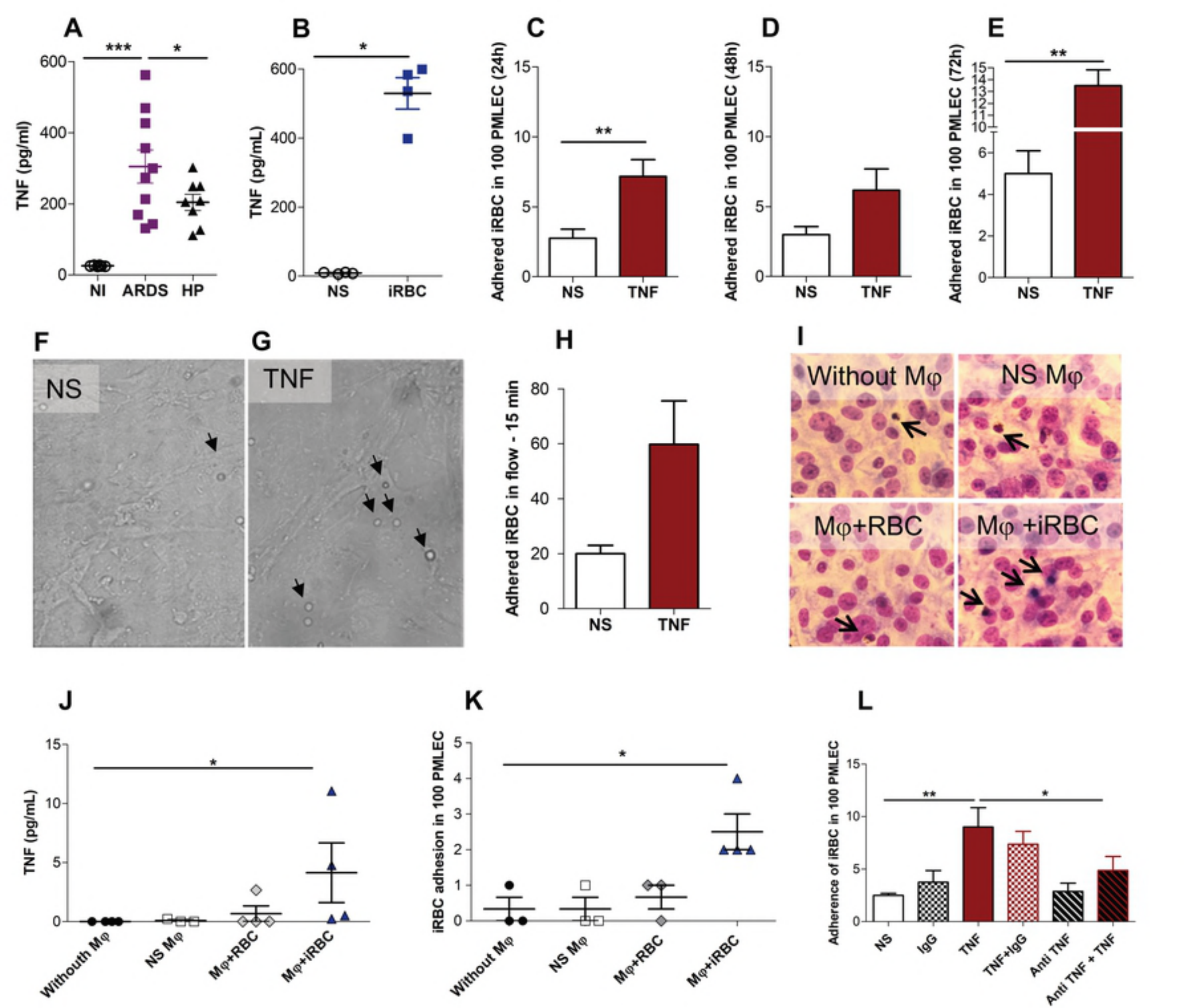
A
TNF (pg/ml)
600
400
200
0
***
*
NI
ARDS
HP
B
TNF (pg/mL)
600
400
200
0
*
NS
iRBC
C
Adhered iRBC in 100 PMLEC (24h)
15
10
5
0
**
NS
TNF
D
Adhered iRBC in 100 PMLEC (48h)
15
10
5
0
NS
TNF
E
Adhered iRBC in 100 PMLEC (72h)
15
14
13
12
11
10
6
4
2
0
**
NS
TNF
F
NS
G
TNF
H
Adhered iRBC in flow - 15 min
80
60
40
20
0
NS
TNF
I
Without Mφ
NS Mφ
Mφ+RBC
Mφ +iRBC
J
TNF (pg/mL)
15
10
5
0
*
Withouth Mφ
NS Mφ
Mφ+RBC
Mφ+iRBC
K
iRBC adhesion in 100 PMLEC
5
4
3
2
1
0
*
Without Mφ
NS Mφ
Mφ+RBC
Mφ+iRBC
L
Adherence of iRBC in 100 PMLEC
15
10
5
0
**
*
NS
IgG
TNF
TNF+IgG
Anti TNF
Anti TNF + TNF

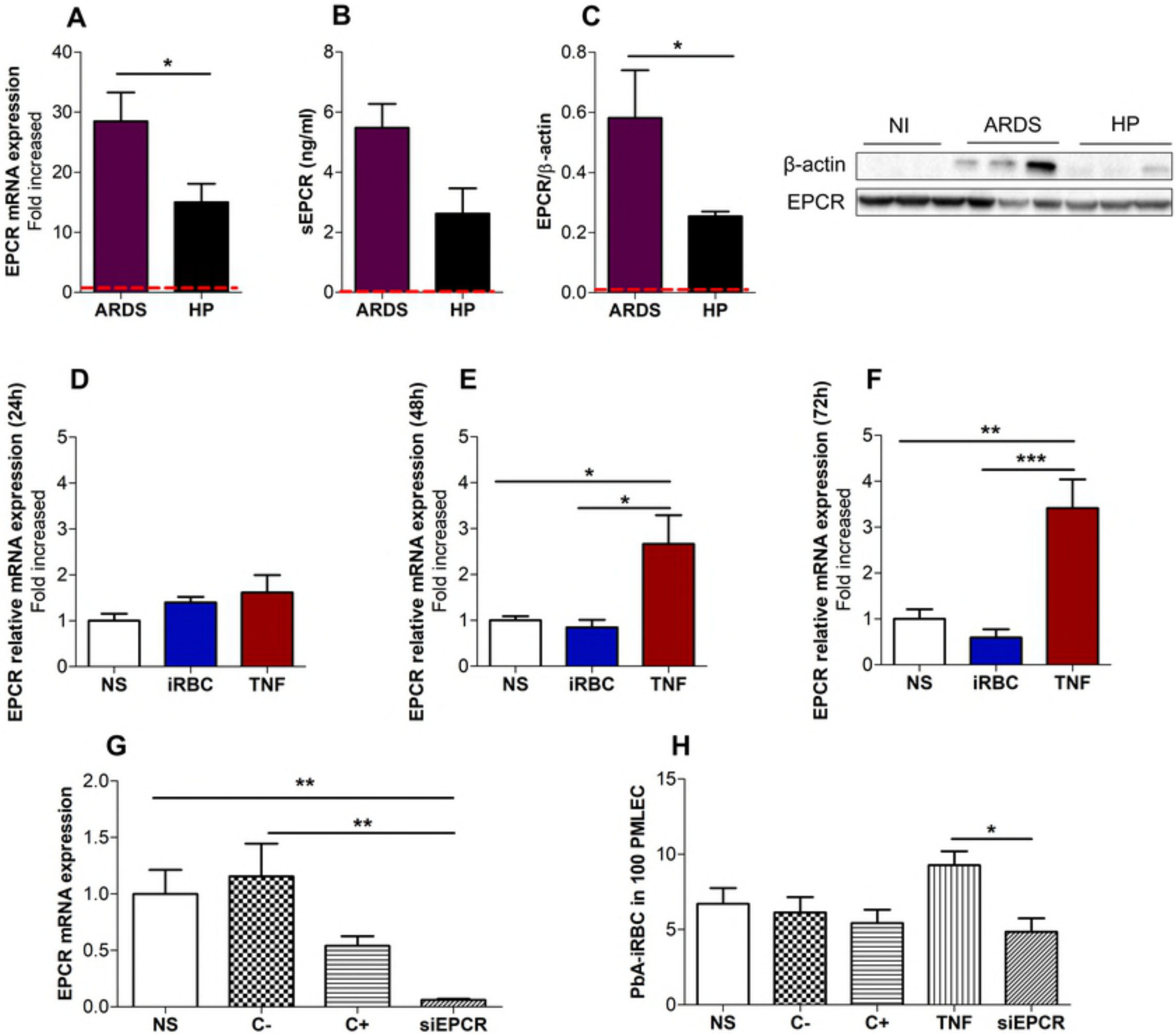
A
EPCR mRNA expression
Fold increased
40
30
20
10
0
*
ARDS
HP
B
sEPCR (ng/ml)
8
6
4
2
0
ARDS
HP
C
EPCR/β-actin
0.8
0.6
0.4
0.2
0.0
*
ARDS
HP
NI
ARDS
HP
β-actin
EPCR
D
EPCR relative mRNA expression (24h)
Fold increased
5
4
3
2
1
0
NS
iRBC
TNF
E
EPCR relative mRNA expression (48h)
Fold increased
5
4
3
2
1
0
*
*
NS
iRBC
TNF
F
EPCR relative mRNA expression (72h)
Fold increased
5
4
3
2
1
0
**
***
NS
iRBC
TNF
G
EPCR mRNA expression
2.0
1.5
1.0
0.5
0.0
**
**
NS
C-
C+
siEPCR
H
PbA-iRBC in 100 PMLEC
15
10
5
0
*
NS
C-
C+
TNF
siEPCR

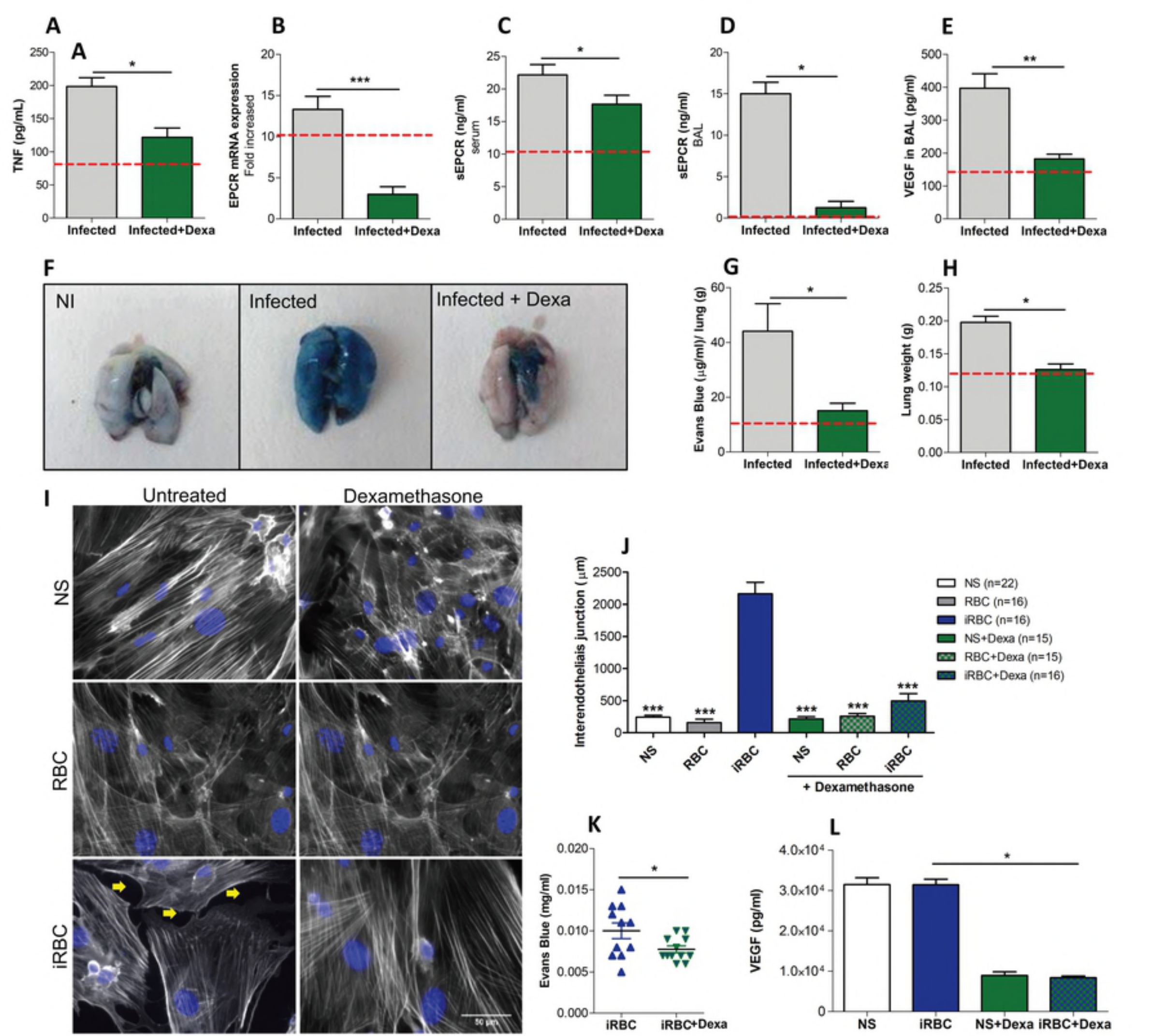
A
TNF (pg/mL)
Infected
Infected+Dexa
B
EPCR mRNA expression
Fold increased
C
sEPCR (ng/ml)
serum
D
sEPCR (ng/ml)
BAL
E
VEGF in BAL (pg/ml)
F
NI
Infected
Infected + Dexa
G
Evans Blue (µg/ml)/ lung (g)
H
Lung weight (g)
I
Untreated
Dexamethasone
NS
RBC
iRBC
J
Interendotheliais junction (µm)
NS (n=22)
RBC (n=16)
iRBC (n=16)
NS+Dexa (n=15)
RBC+Dexa (n=15)
iRBC+Dexa (n=16)
+ Dexamethasone
K
Evans Blue (mg/ml)
iRBC+Dexa
L
VEGF (pg/ml)
NS+Dexa

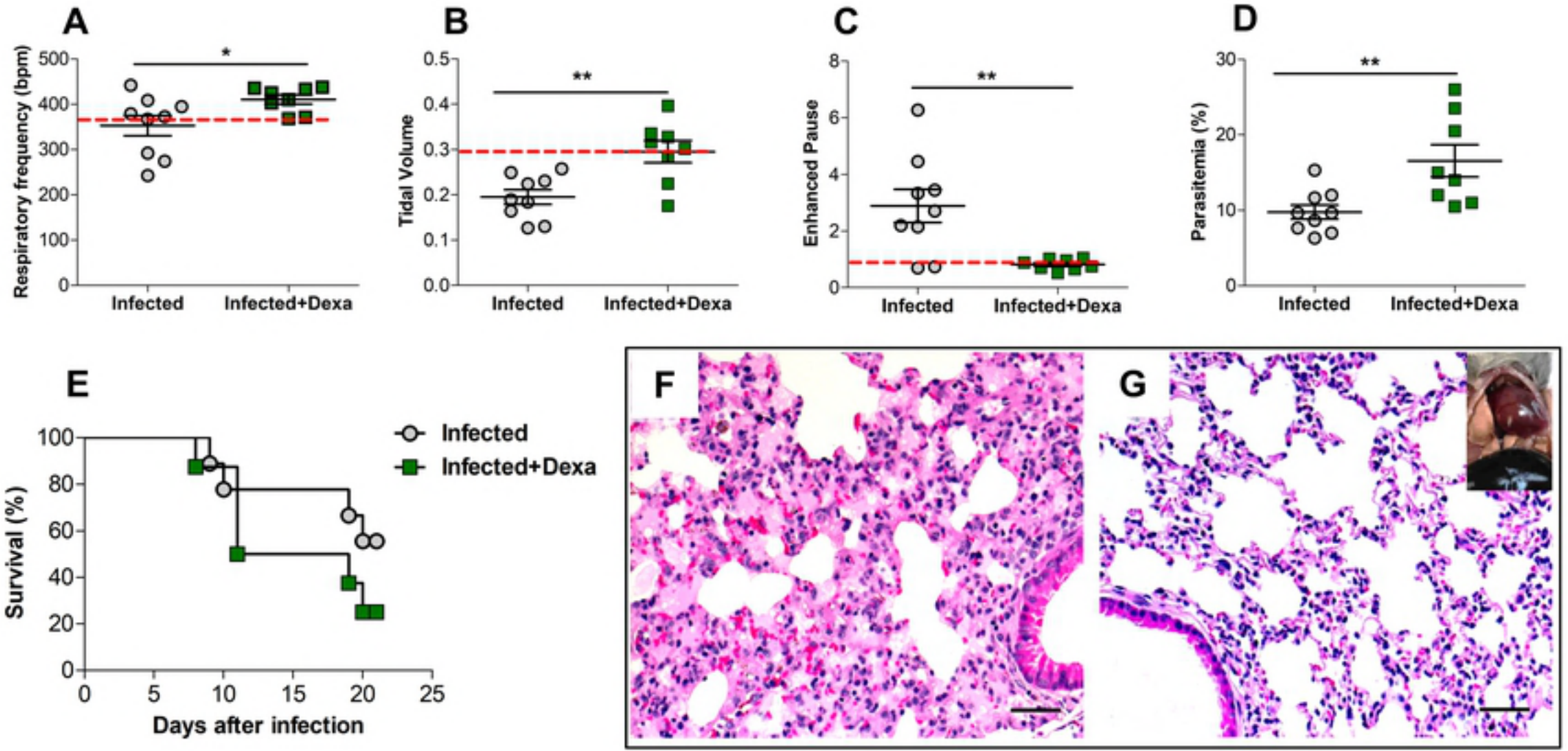
A
Respiratory frequency (bpm)
500
400
300
200
100
0
*
Infected
Infected+Dexa
B
Tidal Volume
0.5
0.4
0.3
0.2
0.1
0.0
**
Infected
Infected+Dexa
C
Enhanced Pause
8
6
4
2
0
**
Infected
Infected+Dexa
D
Parasitemia (%)
30
20
10
0
**
Infected
Infected+Dexa
E
Survival (%)
100
80
60
40
20
0
0
5
10
15
20
25
Days after infection
Infected
Infected+Dexa
F
G

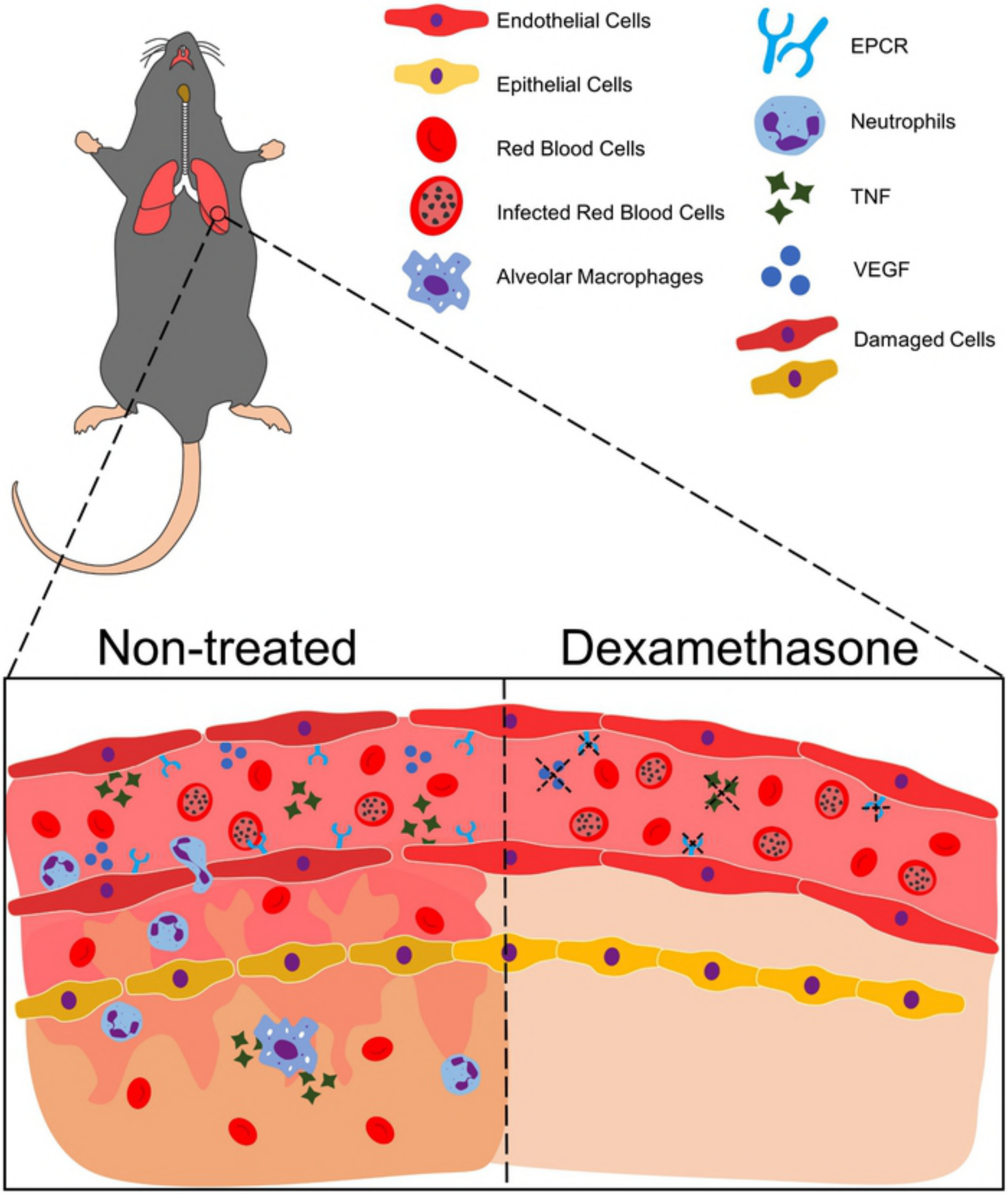
Endothelial Cells
Epithelial Cells
Red Blood Cells
Infected Red Blood Cells
Alveolar Macrophages
EPCR
Neutrophils
TNF
VEGF
Damaged Cells
Non-treated
Dexamethasone